

er than within days. Volumes of the Plexiglas (acrylic plastic) measurement chambers were 0.02 m<sup>3</sup> for 0.09-m<sup>2</sup> plots and 0.1 m<sup>3</sup> for 0.2-m<sup>2</sup> plots. The 4.4-m<sup>3</sup> chambers for the 6.25-m<sup>2</sup> plots had permanent walls and a temporary plastic roof. CO<sub>2</sub> measurements were made with a LICOR 6200 portable infrared gas analyzer (7, 8). Measurement duration averaged 60 s, with a chamber effect on temperature (<2°C) only during periods of direct solar radiation. Because of the small magnitude of the temperature change, the small effect of temperature on flux (see results), and a study design that measured fluxes from disturbed and undisturbed sites under similar conditions, any biases due to chamber effects are probably small. Fluxes measured with an aerodynamic method, based on the vertical profile of

CO<sub>2</sub> concentration and wind speed [J. L. Monteith and M. H. Unsworth, *Principles of Environmental Physics* (Hodder and Stoughton, London, 1990)], gave identical seasonal amplitudes of net CO<sub>2</sub> flux to chamber measurements (S. A. Zimov *et al.*, data not shown), validating our chamber technique. In winter, we used a water jacket to stabilize the temperature of the gas analyzer.

27. We estimate the area-weighted average high-latitude carbon uptake ( $U$ ) as  $U = A_d(F_d) + (1 - A_d)(F_u)$ , where  $A_d = A_b(T)$ .  $F_d$  is the average summer carbon uptake by disturbed ecosystems (186.7 g C m<sup>-2</sup> year<sup>-1</sup>; Table 1);  $F_u$  is the average summer carbon uptake by undisturbed ecosystems (74.3 g C m<sup>-2</sup> year<sup>-1</sup>);  $A_b$  is the proportion of the North American boreal zone burned annually [0.21% in 1960s, 0.57%

in 1990s (20)]; and  $T$  is 30 years, the time a disturbed site is dominated by early successional vegetation (27).  $U$  increased 15% from the 1960s to the 1990s. The average circumpolar changes in disturbance ( $A_b$ ) and recovery rates ( $T$ ) are unknown, so this calculation is only illustrative.

28. We thank I. Fung, J. Gruenzweig, J. Harte, A. McGuire, and J. Randerson for critical review of the manuscript. This research collaboration was funded by the Russian Fund for Fundamental Research, the International Science Foundation, the U.S. Department of Energy, and the Arctic System Science (ARCSS), the Long-Term Ecological Research (LTER), and the Terrestrial Ecosystems and Global Change (TECO) Programs of NSF.

15 December 1998; accepted 4 May 1999

## Xyloglucan Fucosyltransferase, an Enzyme Involved in Plant Cell Wall Biosynthesis

Robyn M. Perrin,<sup>1,2\*</sup> Amy E. DeRocher,<sup>1\*</sup> Maor Bar-Peled,<sup>1,\*†</sup> Weiqing Zeng,<sup>1,4</sup> Lorena Norambuena,<sup>5</sup> Ariel Orellana,<sup>5</sup> Natasha V. Raikhel,<sup>1,3‡</sup> Kenneth Keegstra<sup>1,2,3‡</sup>

Cell walls are crucial for development, signal transduction, and disease resistance in plants. Cell walls are made of cellulose, hemicelluloses, and pectins. Xyloglucan (XG), the principal load-bearing hemicellulose of dicotyledonous plants, has a terminal fucosyl residue. A 60-kilodalton fucosyltransferase (FTase) that adds this residue was purified from pea epicotyls. Peptide sequence information from the pea FTase allowed the cloning of a homologue gene, *AtFT1*, from *Arabidopsis*. Antibodies raised against recombinant AtFTase immunoprecipitate FTase enzyme activity from solubilized *Arabidopsis* membrane proteins, and *AtFT1* expressed in mammalian COS cells results in the presence of XG FTase activity in these cells.

In most multicellular organisms, cells are embedded in a complex extracellular matrix that keeps them together and influences the shape, development, and polarity of the cells they contact. Animal cells have such an extracellular matrix at their surface, but plants possess a distinct wall that encloses every cell. Many important differences between plants and animals with respect to nutrition, growth, reproduction, and defense mechanisms can be traced to the plant cell wall (1). Cell wall extensibility is a major determinant of plant growth (2). The biosynthesis of plant cell walls is very tightly regulated. Although an individual plant cell may expand its volume by nearly 20,000 times,

its cell wall must maintain a uniform thickness and structure to prevent hemorrhaging of the cell through local defects (2). However, despite extensive descriptions of the chemical and physical structure of the plant cell wall, very little is known about its biosynthesis. One gene encoding a cell wall-synthesizing enzyme, cellulose synthase, has been cloned (3).

The flexible primary walls of young plant cells are mainly composed of cellulose microfibrils and matrix polysaccharides. Matrix polysaccharides include hemicelluloses that bind tightly but noncovalently to cellulose microfibrils, cross-linking them into a complex network. The hemicellulose xyloglucan (XG) makes up approximately 20% of the total cell wall in dicot and nongraminaceous monocot plants and forms a load-bearing network by associating to the surfaces of surrounding cellulose microfibrils through hydrogen bonds (4, 5). XG contains a  $\beta$ -1,4-glucan backbone decorated with side chains of xylose alone; xylose and galactose; and xylose, galactose, and fucose. The presence or absence of the terminal fucose residue may have structural and biological significance. Some models suggest that the presence or absence of this fucose residue will determine whether the xyloglucan conformation is planar and thus better able to bind to

cellulose (6), though contradicting evidence has been described (7). XG networks may be modified by XG endotransglycosylase (XET), an enzyme that cleaves and rejoins adjacent XG chains. A recombinant XET demonstrated different activity rates for fucosylated versus nonfucosylated XG oligosaccharide acceptors, indicating that the fucosylation state may affect XET modification of the cell wall (8). In addition, oligosaccharides consisting of an XG nonasaccharide prevent auxin-promoted elongation of pea stems if these oligosaccharides contain fucose but not if they lack fucose (9). Thus, it is possible that XG fragments act as signaling molecules *in vivo*.

Most matrix polysaccharides are branched molecules modified by various sugars. These modifications are important because they allow heterogeneity in the shape of matrix polysaccharides and in the patterns of cross-links, resulting in a dynamic and porous cell wall. These polysaccharide modifications occur via glycosyltransferase reactions, many of which occur in the Golgi complex (10). Attempts to clone plant glycosyltransferases using sequences derived from bacterial or mammalian transferases have been unsuccessful (11). This is not entirely unexpected, for although Golgi glycosyltransferases often have similar general structural features, they rarely share extensive sequence similarity (12).

The terminal fucosyl residue on XG side chains is added by a fucosyltransferase (FTase). We purified enough of this FTase from pea epicotyls to determine partial amino acid sequences from the enzyme. Microsomes were prepared from the pea epicotyls, carbonate-washed to enrich for membrane proteins (13), and solubilized with nonionic detergent such as Triton X-100. A specific assay for this enzyme was developed using tamarind or nasturtium seed storage XG, which lack fucosyl residues, as acceptor molecules and radiolabeled guanosine diphosphate (GDP)-fucose as a donor (14, 15). GDP-agarose affinity chromatography, size exclusion chromatography, and anion exchange chromatography were used in conjunction with FTase activity assays to purify and detect the enzyme (Fig. 1) (16). It was possible to purify XG FTase 1400-fold after size exclusion chromatography, resulting in a total of 50  $\mu$ g of

<sup>1</sup>Michigan State University—Department of Energy (MSU-DOE) Plant Research Laboratory, <sup>2</sup>Department of Botany and Plant Pathology, <sup>3</sup>Department of Biochemistry, <sup>4</sup>Cell and Molecular Biology Program, Michigan State University, East Lansing, MI 48824, USA. <sup>5</sup>Department of Biology, Faculty of Sciences, University of Chile, Santiago, Chile.

\*These authors contributed equally to this work.

†Present address: Monsanto, St. Louis, MO 63198, USA.

‡To whom correspondence should be addressed at MSU-DOE Plant Research Laboratory, Michigan State University, East Lansing, MI 48824, USA. E-mail: nraikhel@pilot.msu.edu (N.V.R.); keegstra@pilot.msu.edu (K.K.)

## REPORTS

protein containing 70 nanokats (nKat) (nanomoles of substrate incorporated into the product per second) of XG FTase activity. To confirm that the purified pea protein synthesizes an  $\alpha$ -1,2 fucose: galactose linkage, carbohydrate analysis was performed on the product resulting from *in vitro* fucosylation of tamarind XG by purified FTase (Table 1) (17). Linkage analysis indicated that incubation of tamarind XG with purified FTase resulted in a decrease in the mole percentage of terminal galactose and the appearance of 2-galactose and terminal fucose, thus verifying the activity of the purified enzyme (Table 1). After biochemical purification and subsequent analysis, two polypeptides of approximately 65 and 60 kD in size were observed to copurify with XG FTase activity (Fig. 1).

Limited peptide sequences were obtained from both proteins (18). The 65-kD peptide was identified as a homolog of BiP, a molecular chaperone usually localized to the endoplasmic reticulum. It remains unclear whether copurification of BiP with FTase represents an important interaction. Six peptides analyzed from the 60-kD protein were not significantly similar to proteins of known function in databases but did allow the identification of an *Arabidopsis* expressed sequence tag (EST), the sequence of which encoded four out of the six peptides, with amino acid identity ranging from 63 to 85% (18).

An analysis of this EST (number 191A6T7) indicated that it was not a full-length clone (19). The EST was used as a probe to screen

an *Arabidopsis* cDNA library, and full-length cDNA clones were isolated (19). The cDNA clones contain a 1677-nucleotide open reading frame encoding a 63.5-kD protein and correspond to a region of the fully sequenced *Arabidopsis* bacterial artificial chromosome (BAC) T18E12 (20). The cDNA and the corresponding genomic clone have been designated *AtFT1*. Analysis of the BAC indicates that there may be a second glycosyltransferase approximately 300 base pairs downstream from *AtFT1* that is 63% similar to *AtFT1* at the amino acid level. In addition, two other *Arabidopsis* ESTs and three *Arabidopsis* genomic sequences that show significant similarity to *AtFT1* have been observed in the databases (21). Thus, *Arabidopsis* may carry a family of FTases, each differentially regulated by such factors as environmental stress, tissue localization, or developmental stage, or specific to different acceptors.

To confirm the identity of *AtFT1* as encoding a fucosyltransferase using XG as an acceptor, we prepared polyclonal antibodies directed against *AtFT1* overexpressed in *Escherichia coli* and used them to immunoprecipitate proteins from carbonate-washed, detergent-solubilized *Arabidopsis* proteins (22, 23). The immunoprecipitated proteins were then assayed for XG FTase activity; 2.6-fold more FTase activity was correlated with pellets derived from immunoprecipitation reactions using immune antiserum rather than preimmune serum, thereby confirming that the *Arabidopsis* clone encodes a XG FTase (Fig. 2). In addition, a COS cell line expressing *AtFT1* showed *in vitro* FTase activity that was 41 times higher than that of COS cells transformed with an empty vector (Fig. 2) (24). Taken together, these data indicate that *AtFT1* is involved in XG biosynthesis.

Although *AtFT1* has some structural characteristics common to other fucosyltransferases, it is quite divergent at the amino acid sequence level. Hydrophobicity plots predict that there may be an  $\text{NH}_2$ -terminal transmembrane signal anchor sequence. *In vitro* translation in the presence of canine pancreatic microsomes followed by carbonate washing of the products indicates that the *AtFT1* translation product is a

**Fig. 1.** Biochemical purification of XG FTase from pea. (A) Silver-stained SDS-PAGE gels showing protein profiles from (i) carbonate-washed detergent-solubilized microsomes from pea epicotyls (Sol. Microsomes) or the fractions containing peaks of FTase activity from (ii) a GDP-agarose affinity column (GDP-affinity) or (iii) a size exclusion column (Size Excl.). Numbers at left indicate sizes in kilodaltons. (B) Top: Silver-stained SDS-PAGE gel showing the protein profile from several fractions of an anion exchange column. Numbers at left indicate sizes in kilodaltons. Bottom: Total XG FTase activity for each fraction of the anion exchange column eluate. Bars align with the corresponding SDS-PAGE profiles above.

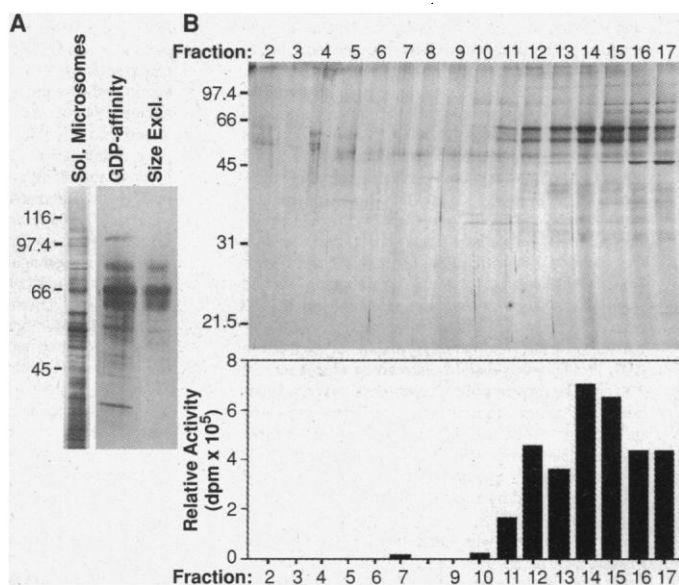


**Fig. 2.** Confirmation of *AtFT1* activity. (A) Polyclonal antibodies to *AtFT1* recognize an approximately 63-kD polypeptide in solubilized membrane proteins of *Arabidopsis*. Top: Left two lanes, immunoblot; right two lanes, Coomassie blue staining of immunoblot membrane. In both cases, lane 1 is *Arabidopsis* carbonate-washed, detergent-solubilized membrane proteins, and lane 2 is antigen (50 ng). Bottom: Antibodies to FTase immunoprecipitate more XG-specific FTase activity than does an equal volume of preimmune serum. The FTase activity of precipitated pellets is shown. This is an example similar to results seen in seven different replicates. (B) Full-length *AtFT1* expressed in a Cos cell line shows XG-specific FTase activity. Activity is shown in the presence (+XG) or absence (-XG) of tamarind XG for untransformed Cos-7 cells, cells transformed with vector DNA (Cos-7 vector), cells transformed with vector containing *AtFT1* (Cos-7 vector *AtFT1*), or solubilized pea Golgi vesicles (Pea Golgi). In graphs, error bars show  $\pm 1$  SD; if no error bars are visible, SDs are contained within the width of the plot element.

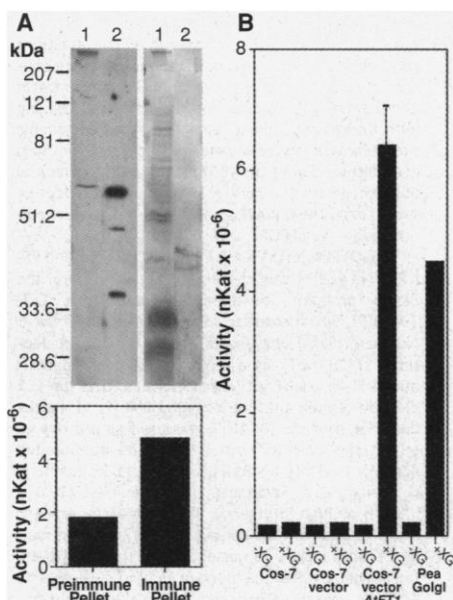


**Table 1.** Carbohydrate linkage analysis of tamarind XG before (tamarind XG) and after (fucosylated XG) incubation with purified pea FTase (17). Dashes indicate that no such linkage was detected.

Sugar residue	Tamarind XG (%)	Fucosylated XG (%)
4-glucose	16.4	17.5
4,6-glucose	37.0	31.5
Terminal xylose	19.0	13.5
2-xylose	15.0	14.3
Terminal galactose	12.6	5.5
2-galactose	—	9.0
Terminal fucose	—	8.7

membrane protein (25). As with other glycosyltransferases, the COOH-terminal region is predicted to be largely hydrophilic. AtFT1 is not significantly similar to any other FTases from other organisms, although multiple sequence alignments have identified three motifs that appear to be conserved among all  $\alpha$ 1,2- FTases (26). One of these motifs, described previously, is found in all  $\alpha$ 1,2- and  $\alpha$ 1,6-FTases for which sequence data are known (27). Because these proteins have different acceptor molecules but share the same sugar nucleotide donor (GDP-fucose), it is possible that these regions are involved in GDP-fucose binding or conserved structural characteristics. Some small regions of similarity are observed between AtFT1 and NodZ, a fucosyltransferase in *Rhizobium* involved in the synthesis of nodulation factors.

The unique nature of this FTase will allow its use as a tool for identifying other plant-specific glycosyltransferases. Hundreds to thousands of different genes (28) are needed to synthesize the various polysaccharides that compose the cell wall. Substrate acceptors and assays remain unavailable for many of these enzymes. Identification of other carbohydrate transferases, perhaps by sequence similarity, could lead to tailored in vitro production of carbohydrates as well as an understanding of how the complex plant cell wall is biosynthesized.

References and Notes

1. N. Carpita, in *Plant Metabolism*, D. Dennis, D. Turpin, D. Lefebvre, D. Layzell, Eds. (Longman, Singapore, ed. 2, 1997), chap. 9.
2. D. J. Cosgrove, *Annu. Rev. Cell Dev. Biol.* **13**, 171 (1997); *Plant Physiol.* **102**, 1 (1993).
3. T. Arioli et al., *Science* **279**, 717 (1998); J. R. Pear, Y. Kawagoe, W. E. Schreckengost, D. P. Delmer, *Proc. Natl. Acad. Sci. U.S.A.* **93**, 12637 (1996).
4. T. Hayashi, *Annu. Rev. Plant Phys. Plant Mol. Biol.* **40**, 139 (1989).
5. E. Zablackis, J. Huang, B. Muller, A. G. Darvill, P. Albersheim, *Plant Physiol.* **107**, 1129 (1995).
6. S. Levy, G. MacLachlan, L. A. Staehelin, *Plant J.* **11**, 373 (1997); S. Levy, W. S. York, R. Struike-Prill, B. Meyer, L. A. Staehelin, *ibid.* **1**, 195 (1991).
7. S. E. C. Whitney, J. E. Brigham, A. H. Darke, J. S. Grant Reid, M. J. Gidley, *ibid.* **8**, 491 (1995).
8. M. M. Purugganan, J. Braam, S. C. Fry, *Plant Physiol.* **115**, 181 (1997).
9. R. A. Creelman and J. E. Mullet, *Plant Cell* **9**, 1211 (1997); S. C. Fry, S. Aldington, P. R. Hetherington, J. Aitken, *Plant Physiol.* **103**, 1 (1993); G. J. McDougall and S. C. Fry, *J. Exp. Bot.* **40**, 233 (1989); W. S. York, A. G. Darvill, P. Albersheim, *Plant Physiol.* **75**, 295 (1984).
10. K. J. Colley, *Glycobiology* **7**, 1 (1997); J. Puhlmann et al., *Plant Physiol.* **104**, 699 (1994); A. Driouich, L. Faye, L. A. Staehelin, *Trends Biochem. Sci.* **18**, 210 (1993); P. J. Moore, K. M. M. Swords, M. A. Lynch, L. A. Staehelin, *J. Cell Biol.* **112**, 589 (1991).
11. A. E. DeRocher, N. V. Raikhel, K. Keegstra, data not shown.
12. R. Kleene and E. G. Berger, *Biochem. Biophys. Acta* **1154**, 283 (1993).
13. Y. Fujiki, A. L. Hubbard, S. Fowler, P. B. Lazarow, *J. Cell Biol.* **93**, 97 (1982).
14. V. Farkas and G. MacLachlan, *Arch. Biochem. Biophys.* **264**, 48 (1988); A. Camirand, D. Brummell, G. MacLachlan, *Plant Physiol.* **84**, 753 (1987).

15. Samples were incubated at room temperature for 20 min (for immunoprecipitation samples) or 30 min (for protein purification samples) with 25 mM Pipes-KOH (pH 6.2), tamarind XG (0.5 mg/ml), and GDP-[<sup>3</sup>H]-fucose to a final concentration of 3.3 nM (573 GBq/mmol; NEN, Boston, MA). Most assays also contained 50  $\mu$ M nonradiolabeled GDP-fucose. Assays of immunoprecipitation samples also contained 5 mM MgCl<sub>2</sub>. Reactions were precipitated with 70% ethanol, and <sup>3</sup>H incorporation was measured by scintillation counting. The amount of fucose incorporated into the product was used to calculate activity in nanokats.
16. Two-centimeter segments, excised just below the apical hook of etiolated *Pisum sativum*, cv Alaska, were collected and homogenized in 1.5 volumes of buffer [50 mM Hepes (pH 7.5); 1 mM EDTA (pH 8.0); 0.4 M sucrose; 1 mM dithiothreitol (DTT); 0.1 mM phenylmethylsulfonyl fluoride (PMSF); and 1  $\mu$ g each of aprotinin, leupeptin, and pepstatin per milliliter]. The homogenate was filtered and centrifuged at 2,000g for 15 min, and the supernatant was centrifuged at 100,000g for 1 hour. The resulting pellets were washed and homogenized in the presence of 0.1 M Na<sub>2</sub>CO<sub>3</sub> to strip away peripheral membrane proteins (73). The suspension was centrifuged at 100,000g for 1 hour, and the resulting pellets were washed and resuspended in buffer [50 mM Pipes-KOH (pH 6.2), 20% glycerol, 1 mM EDTA, 1 mM DTT, 0.1 M PMSF, and 1  $\mu$ g each of aprotinin, leupeptin, and pepstatin per milliliter]. The suspension was homogenized, Triton X-100 was added to a final volume of 0.8%, and the sample was stirred for 1 to 2 hours to solubilize membrane proteins before centrifugation a final time at 100,000g for 1 hour. Supernatant was collected and saved. When *Arabidopsis* cell suspension culture was used as a tissue source, the procedure was identical except that the cells were lysed with a French pressure cell at 4000 psi. Pea carbonate-washed supernatants were pooled and separated on a GDP agarose affinity chromatography column, and GDP-binding proteins were eluted by means of excess free GDP. Protein levels were monitored by absorbance at 280 nm. The protein samples were desalted on a Sephadex G-25 column, concentrated, and further separated on a Phenomenex SEC 4000 size exclusion column. Some samples were further purified with a Poros QE or Resource Q anion exchange column and were subsequently separated by SDS-polyacrylamide gel electrophoresis (SDS-PAGE).
17. Tamarind seed XG was fucosylated by purified pea FTase equal to 33 pKat total activity [assay conditions were as follows: tamarind XG (1 ng/ml), 1.5 mM GDP-fucose, and 50 mM Pipes-KOH (pH 6.2)]. The XG product was precipitated with ethanol, resuspended in water, reprecipitated, and sent to the Complex Carbohydrate Research Center (Athens, GA) for linkage analysis. An equal amount of tamarind XG was also submitted for linkage analysis.
18. Proteins in size exclusion column eluate fractions containing peak amounts of FTase activity were concentrated with a Millipore 4-ml 10-kD concentrator and separated by electrophoresis. After brief staining with Coomassie brilliant blue R250 and destaining, the separated proteins were excised, rinsed in 50% acetonitrile, stored at -80°C, and sent to Harvard Microchemistry (Cambridge, MA) for tryptic peptide sequencing. The following six peptide sequences were obtained: VFGFLGR, YLLHPTNNVWGLVPR, AV-LITSLSSGYFEK, YYDAYLAK, LLGLLADGFDEK, and ES-ILPDVNR (29). Using these peptides as a query, the Blastp program identified an *Arabidopsis* EST, 191A677, which encoded four out of six peptides.
19. Northern (RNA) blot analysis using the 858-nucleotide EST 191A677 as a probe detected an approximately 2-kb transcript, which indicates that the EST did not contain the full-length cDNA (R. M. Perrin, data not shown). 191A677 was used as a probe to screen the CD4-15 portion of a size-fractionated *Arabidopsis* cDNA library [J. J. Kieber, M. Rothenberg, G. Roman, K. A. Feldmann, J. R. Ecker, *Cell* **72**, 427 (1993)] at high stringency. Two cDNA clones were isolated, the longest containing a 1768-base pair insert. Both lacked 13 nucleotides of the 3' UTR and the polyadenylated tail found in 191A677. There is an AATAAA consensus polyadenylation signal eight nu-

cleotides from the 3' end of the library-derived clones. The sequence contains a 1677-nucleotide open reading frame that encodes a 63.5-kD protein. The translation product also contains a region near the NH<sub>2</sub>-terminus that is similar to a fifth pea peptide (78). The nucleotide sequence of AtFT1 has been assigned the GenBank accession number AF154111.

20. AtFT1 is encoded within BAC T18E12, derived from chromosome II (nucleotides 41209 through 41503 and 41780 through 43252), which has been fully sequenced by the *Arabidopsis* Genome Initiative. A second open reading frame has been predicted within T18E12 (nucleotides 43562 through 43748 and 43813 through 45215), which shows 63% similarity to AtFT1 at the deduced amino acid level.
21. R. M. Perrin, N. V. Raikhel, K. Keegstra, C. Wilkerson, unpublished results.
22. The portion of AtFT1 encoding amino acids 73 through 566 was amplified by polymerase chain reaction using appropriate primers and cloned into the pET28a expression vector (Novagen, Madison, WI). The resulting insoluble fusion protein was purified by washing of inclusion bodies four times with 1% Triton X-100, 50 mM Hepes-KOH (pH 7.6), and 10 mM MgCl<sub>2</sub> and washing one time with 25 mM Hepes-KOH (pH 7.0) and 8 M urea. The pellet was resuspended in 6 M guanidine-HCl, and protein was precipitated from the supernatant with 10% trichloroacetic acid. The protein was emulsified with Titermax adjuvant (CytRx Corporation, Norcross, GA) and injected into a rabbit. For protein immunoblotting, 40  $\mu$ l of carbonate-washed solubilized protein from *Arabidopsis* and 50 ng of purified antigen were separated by SDS-PAGE and electroblotted. Antibodies to AtFT1 (dilution, 1:5000) were used for protein immunoblotting. Horseradish peroxidase-conjugated goat antibodies raised against rabbit antibodies were used as secondary antibodies. Signals were detected by the enhanced chemiluminescence method (Pierce, Rockford, IL). Membranes were stained with Coomassie blue to detect protein.
23. For immunoprecipitations, solid NaCl was added to carbonate-washed solubilized *Arabidopsis* protein to a final concentration of 200 mM. The *Arabidopsis* protein was precleared by incubation with 1:10 volume of a 50% slurry of protein A-Sepharose beads (Pharmacia) in buffer A [25 mM Pipes-KOH (pH 7.5), 50 mM NaCl, and 2 mM EDTA (pH 8.0)]. The resulting supernatants were incubated with 50  $\mu$ l of immune or preimmune antiserum to AtFT1 for 1 hour. A 1:5 volume of protein A-Sepharose slurry was added to precipitate the antigen-antibody complexes, and the samples were incubated for an additional 3 hours with rocking at 4°C. Samples were then centrifuged and washed five times in buffer A containing 1% Triton X-100 and two times in buffer A without detergent. The pellets were resuspended in buffer A to a final volume of 120  $\mu$ l and assayed for AtFTase activity as described above.
24. Cos-7 cells were grown on 100-mm plates in Dulbecco's modified Eagle's medium (DMEM) and 10% fetal bovine serum. Cells were transfected with different plasmids using Lipofectamine reagent (Life Technologies) according to the manufacturer's instructions, using 9  $\mu$ g of DNA and 72  $\mu$ g of Lipofectamine. Cells were incubated for 24 hours in the medium containing DNA and Lipofectamine without fetal bovine serum. The medium was then changed to DMEM plus 10% fetal bovine serum and incubated for another 48 hours. The cells were scraped off the dish in 0.25 M sucrose, 10 mM tris-HCl (pH 7.5), and 0.4% CHAPS. XG-FTase activity was measured with 50  $\mu$ g of protein in the absence or presence of 100  $\mu$ g of tamarind XG. The incubation was carried out in a volume of 0.1 ml in the presence of 1  $\mu$ M GDP-fucose (93,000 disintegrations per minute), 10 mM MnCl<sub>2</sub>, 20 mM Hepes (pH 7.0), and 0.05% Triton X-100 at 25°C for 90 min. The reaction was halted by the addition of ethanol to a final concentration of 70%. Samples were incubated at 4°C and filtered through 1.5- $\mu$ m glass fiber filters. The filters were washed with 70% ethanol containing 1 mM EDTA. The filters were then dried and radioactivity was determined by liquid scintillation. A biological control using pea Golgi vesicles was carried out in parallel.

## REPORTS

25. R. M. Perrin, K. Keegstra, N. V. Raikhel, data not shown.
26. Three motifs were found to be conserved among several  $\alpha$ -1,2-fucosyltransferases, despite low overall homology. One ([IV]G[IV][HQ][V]R[DN]) has been described previously (27) (square brackets indicate that either of the indicated amino acids was found at the indicated position; dots indicate that three or more different amino acids were found at the indi-

- cated position). In addition, a second motif (D[EK][MQ][F]F[CR][EQ].DQ) and a third region (G[LF]G[ND][RC][IL].[TS][LI]A[SA].[FW][LR][YF]A.[LQ]T[DG]R.[LA].[VI][DE]) were conserved (29).
27. C. Breton, R. Oriol, A. Inberty, *Glycobiology* **8**, 87 (1998).
28. J. E. Varner and L.-S. Lin, *Cell* **56**, 231 (1989).
29. Single-letter abbreviations for the amino acid residues are as follows: A, Ala; C, Cys; D, Asp; E, Glu; F, Phe; G,

Gly; H, His; I, Ile; K, Lys; L, Leu; M, Met; N, Asn; P, Pro; Q, Gln; R, Arg; S, Ser; T, Thr; V, Val; W, Trp; and Y, Tyr.

30. The authors acknowledge funding from the Department of Energy (grant DE-FG02-91ER20021), C. Wilkerson for assistance with computer analysis, and members of the Keegstra and Raikhel laboratories for helpful discussions.

27 January 1999; accepted 10 May 1999

# Dissociating Pain from Its Anticipation in the Human Brain

Alexander Ploghaus,<sup>1,2\*</sup> Irene Tracey,<sup>1\*</sup> Joseph S. Gati,<sup>3</sup> Stuart Clare,<sup>1</sup> Ravi S. Menon,<sup>3</sup> Paul M. Matthews,<sup>1</sup> J. Nicholas P. Rawlins<sup>2</sup>

The experience of pain is subjectively different from the fear and anxiety caused by threats of pain. Functional magnetic resonance imaging in healthy humans was applied to dissociate neural activation patterns associated with acute pain and its anticipation. Expectation of pain activated sites within the medial frontal lobe, insular cortex, and cerebellum distinct from, but close to, locations mediating pain experience itself. Anticipation of pain can in its own right cause mood changes and behavioral adaptations that exacerbate the suffering experienced by chronic pain patients. Selective manipulations of activity at these sites may offer therapeutic possibilities for treating chronic pain.

Intense, noxious stimulation leads to physiological, emotional, and behavioral changes of obvious adaptive significance (1). One is the experience of pain, which minimizes immediate harm by motivating escape (2). A second is the activation of mechanisms to prevent future harm by learning to recognize signals of impending pain (3), allowing future painful events to be expected and thus avoided.

Functional neuroimaging has previously been used to identify cerebral activation patterns associated with the experience of pain (4, 5). Brain areas activated during peripheral painful stimulation included anterior cingulate, insular, prefrontal and somatosensory cortices, and the thalamus (6). Attempts to discriminate between brain responses associated with the expectation of pain and those associated with the direct experience of pain are only now beginning (7). This distinction is important because not only do these two processes have the separate adaptive consequences outlined above, but they also have potentially separate, maladaptive consequences. For example, expectation of pain by itself may be an important factor in the development of

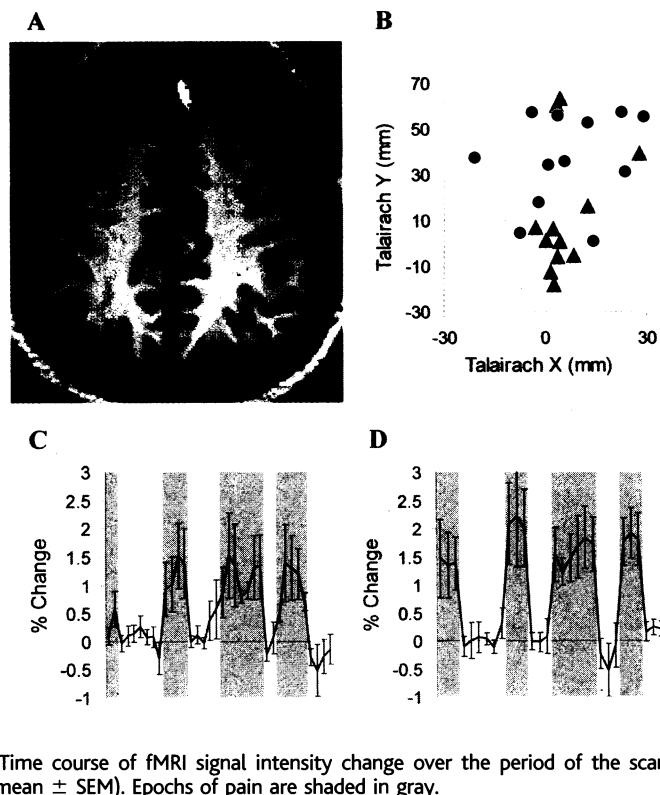
chronic pain syndromes (8). A dissection of the functional neuroanatomies of the expectation and the experience of pain could therefore aid development of therapeutic strategies for the treatment of chronic and acute pain.

Twelve healthy volunteers underwent functional magnetic resonance imaging (fMRI) (9)

while being presented with a pseudo-random sequence of two intensities of thermal stimulation (painful hot or nonpainful warm). Colored lights signaled in advance the two kinds of thermal stimulation. Subjects learned during the imaging session which color signaled pain and which signaled warmth (10). We identified brain regions involved in the experience of pain by comparing brain activation during pain with activation during warm stimulation. This comparison, denoted "pain," controls for somatosensory input unrelated to pain. In addition, we identified brain regions involved in the anticipation of pain by comparing brain activation during the colored light preceding pain to activation during the colored light preceding warm stimulation. This comparison, denoted "anticipation," controls for anticipatory processes unrelated to pain (11).

Interviews after the experiment confirmed that all subjects were aware of the relation between the light color and the intensity of the thermal stimulation. Subjects rated painful heat significantly higher than nonpainful warmth on two 11-point visual analog scales measuring intensity [mean  $\pm$  SD, 7.3  $\pm$  1.3

**Fig. 1.** Medial frontal lobe. (A) Group-combined activation map showing volumes selectively activated during pain (red) and anticipation of pain (yellow). (B) Individual subject's activation centers during pain (red triangles) and anticipation of pain (black circles). Centers associated with the anticipation of pain (black circles; mean Talairach coordinates  $x = 8$  mm,  $y = 38$  mm,  $z = 27$  mm) were significantly more anterior than those associated with pain [red triangles; mean coordinates  $x = 3$  mm,  $y = 4$  mm,  $z = 33$  mm (24)] ( $P < 0.05$ ). (C) Time course of fMRI signal intensity change over the period of the scan averaged across subjects. Epochs related to anticipation of pain are shaded in gray (mean  $\pm$  SEM). (D) Time course of fMRI signal intensity change over the period of the scan averaged across subjects (mean  $\pm$  SEM). Epochs of pain are shaded in gray.



<sup>1</sup>Centre for Functional Magnetic Resonance Imaging of the Brain, Department of Clinical Neurology, University of Oxford, Oxford OX3 9DU, UK. <sup>2</sup>Department of Experimental Psychology, University of Oxford, South Parks Road, Oxford OX1 3UD, UK. <sup>3</sup>Laboratory for Functional Magnetic Resonance Research, John P. Robarts Research Institute, 100 Perth Drive, London, Ontario N6A 5K8, Canada.

\*To whom correspondence should be addressed. E-mail: alex@fmrib.ox.ac.uk, irene@fmrib.ox.ac.uk